Materials Research. 2024; 27:e20230571
DOI: https://doi.org/10.1590/1980-5373-MR-2023-0571

The role of Argon in the AISI 420 Stainless-Steel Low-Temperature Plasma Nitriding

C. J. Scheuer[a,b], R. Pereira[b], R. P. Cardoso[b,c], M. Mafra[b,d], S. F. Brunatto[b]*

[a]*Universidade Federal de Santa Maria, Departamento de Engenharia Mecânica, Santa Maria, RS, Brasil.*
[b]*Universidade Federal do Paraná, Departamento de Engenharia Mecânica, Grupo de Tecnologia de Fabricação Assistida por Plasma e Metalurgia do Pó, Curitiba, PR, Brasil.*
[c]*Universidade Federal de Santa Catarina, Departamento de Engenharia Mecânica, Florianópolis, SC, Brasil.*
[d]*Universidade Tecnológica Federal do Paraná, Departamento Acadêmico de Mecânica, Curitiba, PR, Brasil.*

Received: December 24, 2023; Revised: April 06, 2024; Accepted: April 24, 2024

AISI 420 steel samples were subjected to three heat treatment conditions: annealed, hardened, and tempered at 400°C, followed by low-temperature nitriding using N2, H2, and varying Ar proportions in a pulsed DC glow discharge. The study aimed to investigate the impact of varying Ar content (10–50 vol.%) on glow discharge characteristics and surface properties of nitrided samples, using an 80% N2 + 20% H2 base gas mixture. The samples underwent characterization including optical microscopy, X-ray diffractometry, microhardness, and roughness measurements. Plasma characterization was conducted using optical emission spectroscopy. The results indicated that higher Ar concentrations led to increased thickness of the nitrided layer (up to 67%), as well as hardness (up to 14%) and surface roughness (up to 50%). These improvements stemmed from increased Ar-based species bombardment on the surface, enhancing the cleaning effect of surface oxides. This facilitated nitrogen adsorption onto the steel surface, increasing the atomic nitrogen concentration in the outermost layer of the steel. The increased nitrogen concentration facilitated diffusion, resulting in significant physical-chemical reactions at the surface-plasma interface. These reactions, including sputtering, molecule dissociation, and recombination, led to enhanced high-diffusivity pathways within the martensitic microstructures of both the as-hardened and 400°C-tempered samples.

Keywords: *AISI 420 stainless steel, low-temperature pulsed DC plasma nitriding, argon in nitriding gas mixtures, optical emission spectroscopy, glow discharge (plasma) diagnostics.*

1. Introduction

Plasma nitriding represents a widely adopted technology for surface modification of engineering materials[1-3]. This technique enables the enhancement of mechanical, tribological, and chemical surface properties of metallic alloys while preserving its bulk properties of the substrate[4,5]. Since the 1980s, significant attention has been directed towards advancing plasma nitriding techniques for stainless steels. This heightened focus stems from the inherent advantages offered by plasma-assisted methods over conventional solid and gas nitriding treatments[6]. Presently, plasma-assisted treatments conducted at low temperatures have undergone extensive scrutiny and have experienced a burgeoning application within industrial settings[7-9].

The low temperatures employed in stainless steels treatments decrease the nitriding efficiency due to the reduction of the active nitriding species density[10]. One way to overcome this problem is the proper selection and adjustment of the nitriding gas mixture[11], since the ionization rate is low in pure N_2 plasma due to the highly stable binding strength of N_2 molecule[12]. As such, the gas mixture composition plays important role in order to optimize the surface properties of the nitrided materials. This is based on the fact that the gas dilution, which is a variable directly related to the utilized gas mixture, usually determines the atoms saturation rate available to react with the material surface[13].

It is very well established that the H_2 gas is usually used in addition to N_2 in plasma nitriding gas mixtures, since the hydrogen enhances the rates of N_2 dissociation and the plasma ionization[14]. These effects are due to the fact that hydrogen has a minor collisional cross-section on nitrogen and, additionally, for acting in the removal of the oxide protective layer existing on the stainless steels surface[15,16], which acts as a barrier to nitrogen diffusion. The oxides removal also enhances the emissions of secondary electron and, consequently, the discharge ionization increasing the plasma assisted treatments efficiency[5,17,18]. It is worth mentioning, as shown by some authors[5,19], the ideal proportion of H_2 added to the nitriding gas mixture is about 20%.

In view of evaluation for the metallurgical features of the nitrided material, similarly there are many studies devoted to the analysis of the influence of H_2 ratio on nitriding gas mixture[5,15,20-32]. As can be evidenced in the referred works, there is no agreement on the role of the H_2, since ref[15,25,29,30]. show that by increasing the H_2 content, both the hardness

*e-mail: cristiano.scheuer@ufsm.br

and thickness of the treated layer tend to be also increased. Differently, ref[5,24,26,28,32]. show opposite results, *id. est*, tendency of growth for the nitrided layer hardness and thickness, by decreasing the H_2 content in the gas mixture. In the first case, the greatest nitriding efficiency is credited to the role of hydrogen on the surface oxide layer reduction, and to the increasing active nitriding species density in the plasma. For the second case, the authors claim that the increasing nitriding efficiency is due to the increased nitrogen potential, owing to the smaller H_2 content. Among the referred works, all studies comprising the employment of a pure N_2 atmosphere[24-31], agree well that the use of a N_2 (single gas) plasma is less efficient than those based on H_2-N_2 gas mixtures.

To investigate alternatives to the H_2-N_2 gas mixtures, several studies were performed encompassing other mixtures such as N_2-Ar[13,16,33-44], N_2-H_2-Ar[16,37], N_2-Ne[44], and N_2-O_2-H_2-^{2}H (deuterium)[4]. Particularly, the Ar addition to form a binary mixture with N_2 substantially increases the N active species production through Penning ionization and dissociation processes[16], promoting an increased nitriding efficiency, as verified on different plasma-assisted nitriding systems. In conventional[36], and active screen[37] dc plasma configurations, Ar content additions up to 70 vol.% increase the plasma (electrons or ions) density, its temperature, and the atomic N-based (neutrals, excited and ions) species density, although meaningly reduce the density of molecular ionized species (N_2^+) beyond 30%[38], as it was also observed in the optical emission spectroscopy results obtained here. In rf plasma configuration, it was found that the N_2 dissociation and active species concentration were appreciably enhanced, by rising the Ar content up to 50-60 vol.%, while the concentration of N_2^+ decreased[39]. In the case of inductively coupled discharges[40] and electron cyclotron resonance plasmas[41], it has been observed that the highest rates of N_2 dissociation, and consequently, the peak production of atomic N species, were achieved at approximately 30% and 80% Ar contents, respectively. Such enhancement on atomic N species density due to the Ar addition promoted increased nitrided layers thickness and hardness, as shown in refs[16,33,42,43]. Lastly, regarding N_2-H_2-Ar ternary gas mixtures, it was demonstrated by Naeem et al.[16,37] that Ar contents up to 30% benefit the generation of atomic N- and molecular N_2-based species, promoting the growth of the hardness and wear resistance of the nitrided material.

Investigating the influence of argon concentration in the gas mixture employed for nitriding, particularly concerning AISI 420 martensitic stainless steel (MSS), is paramount due to its widespread usage, especially in environments prone to rapid corrosion and wear[45-48]. The imperative of utilizing surface treatments, such as thermochemical treatments, to enhance the properties and performance of AISI 420 MSS in such environments is crucial for ensuring the durability and reliability of components derived from it[49,50]. Nitriding is a surface treatment process that facilitates the formation of nitrogen-expanded martensitic phase, resulting in substantial enhancements in corrosion and wear resistance of martensitic steels. During nitriding, nitrogen diffuses into the material's surface, forming a hardened layer known as the 'nitrided case'. This layer primarily comprises iron nitrides and nitrogen dissolved in the martensitic matrix[8].

The presence of the nitrogen-expanded martensitic phase, induced by nitriding, imparts superior surface properties to the material, including increased hardness, wear, and corrosion resistance[9]. Thus, nitriding stands as a pivotal process for enhancing performance and extending the lifespan of components manufactured from martensitic steels, significantly contributing to various industrial applications. As previously mentioned, the role of argon in the nitriding atmosphere is significant, impacting the kinetic and thermodynamic reactions of the process. However, there exists a limited comprehension of how argon concentration influences the nitriding behavior of AISI 420 MSS. Therefore, investigating this relationship is essential to optimize process parameters, enhance energy efficiency, and reduce operational costs. Moreover, advancing scientific understanding of gas-solid interactions in metallurgy contributes to the development of more efficient and sustainable surface modification techniques.

Given the limited number of studies, particularly concerning stainless steel substrates, investigating the impact of Ar additions to N_2-H_2-based gas mixtures, the precise role of Ar in enhancing nitriding efficiency remains incompletely understood. To contribute to this area, this study explores the influence of Ar on the plasma nitriding of AISI 420 MSS, examining its effects on both glow discharge characteristics and metallurgical properties of the treated material. Optical emission spectroscopy is employed as a diagnostic tool to gain insights into the formation of reactive species responsible for nitriding. Microstructural features of the nitrided layers are analyzed through optical microscopy, X-ray diffractometry, microhardness, and roughness measurements. The role of Ar in the plasma gas mixture on nitrided layer formation is investigated by integrating results from plasma diagnostics with metallurgical characterization.

2. Experimental Procedures

Cylindrical samples of AISI 420 MSS with 10 mm in height were cut from an 9.5 mm diameter commercial annealed rod (for a composition of 0.17% C, 0.70% Mn, 0.50% Si, 12.2% Cr, 0.23% P, 0.03% S and Fe balance, in wt.%). Part of these samples were austenitized at 1050 °C for 0.5 h and air-cooled to obtain full-martensite (bct) structure. Half of these air-hardened samples were tempered at 400°C for 1 h to acquire tempered-martensite (bcc) structure. These three groups of samples were subsequently ground using SiC sandpaper ranging from 180 to 1200 grade and mirror polished using 1 µm Al_2O_3 abrasive suspension. Posteriorly, samples were cleaned with alcohol in ultrasound bath, dried in a heated airflow, and finally introduced into the discharge chamber. The measured hardness of as-hardened, as-400°C-tempered, and as-annealed samples was 488±12, 421±24, and 327±13 $HV_{0.3}$, respectively.

A pulsed *dc* power supply operating at 4.2 kHz was used to perform the nitriding treatments. The glow discharge was generated using a 600 V pulse (peak) voltage, and the duty cycle was adjusted to obtain the desired temperature (the heating of samples acting as the cathode was provided by plasma species bombardment only). In order to promote ultimate cleaning and aiming to remove the (Cr_2O_3) native oxide layer from the samples surface, prior to the nitriding step, treating samples were sputter-cleaned at 300 °C for 0.5 h in a glow discharge generated using a gas mixture of 80% H_2 + 20% Ar. All plasma nitriding treatments were carried out at 350 °C for 6 h times, employing a gas flow rate of 3.34×10^{-6} Nm^3 s^{-1} (200 sccm), under a pressure of 400 Pa (3 Torr). These parameters were selected based on results obtained in previous studies[51-53]. A scheme and more detailed description of the nitriding plant and procedure can be obtained in ref[51,54].

The choice of a treatment temperature of 350°C was primarily aimed at avoiding the precipitation of chromium nitride phases, which are detrimental to the material's corrosion resistance. Additionally, this temperature was selected because it is sufficiently low to induce significant changes in the material's structure, which could influence the kinetics of the nitriding process. Finally, this temperature is recommended for the tempering of the material in its as-quenched state, allowing for the simultaneous execution of two operations (tempering + nitriding) in a single cycle. In the case of samples that have already been tempered, this temperature is lower than that employed in the previous tempering process and therefore does not exert any additional effect.

To study the effect of Ar on features of the glow discharge and surface properties of the nitrided samples, six-gas mixture compositions were evaluated, which are indicated in Table 1, being also indicated the adopted samples codification. The choice of argon values, ranging proportionally in volume from 0% to 50%, was based on research findings documented in the literature[16,36-43]. These studies indicate that higher argon content improves nitriding efficiency by facilitating the removal of surface oxides from stainless steels and promoting the formation of reactive nitrogen radicals that react with the steel surface. However, these sources also note that argon levels exceeding 50% lead to a decrease in the density of reactive nitrogen species.

In order to evaluate the active species as a function of the Ar content added on the base gas mixture, an experiment was specially specified for optical emission spectroscopy measurements, following a procedure similar to that adopted in ref[52]. The experimental apparatus was equipped with a 2048-element linear silicon CCD array and a 600 lines/mm grating, set to operate on the range of 200-850 nm, presenting a wavelength resolution of 1.5 nm (full width at half maximum). In the related experiments, the Ar content was changed, starting from de gas mixture of 80% N_2 + 20% H_2 (condition #0, in Table 1), and being added for amounts of 10 vol.% up to 50 vol.% Ar to each 60 minutes (see in Table 1, conditions from #10 to #50, respectively). The spectrum was achieved by recording the data to each 5 minutes. For this purpose, the t_{ON} was adjusted as a function of the applied gas mixture, in order to maintain the temperature at 350 °C (623 K). It is to be noted that the experiment was designed this way aiming to ensure the same solid angle, so the emission spectra for each gas mixture condition was acquired without any changes in the experimental setup. As the position between sample and optical fiber was kept unaltered, intensity of the obtained emission lines could be successfully confronted. Five spectra were obtained for each gas mixture condition. The average values indicated for the optical emission spectroscopy data were estimate by the spectrometer software from these five spectra. The respective measurement errors (indicated by error bars on the points of the graphic of optical emission spectroscopy results) were estimated from the standard deviation determined from the two spectra showing the larger measurement data differences for each gas mixture condition.

Nitrided samples were cross-sectioned and prepared for microstructural analysis following the conventional metallographic procedure. After polishing, samples were etched using Vilella's reagent (1 g of picric acid + 4 mL of HCl + 96 mL of ethanol). The etched samples cross-section was analyzed using an Olympus BX51M optical microscope. To identify the phases present in the nitrided layers, Xray diffractometry (XRD) technique was performed using a Shimadzu XDR7000 Xray diffractometer with a Cu K_α Xray tube in the Bragg-Brentano configuration. The samples roughness was evaluated using the profilometry module of an Olympus LEXT OLS 3000 confocal laser scanning microscope (CLSM), same equipment used to analyze the nitrided surfaces morphology. Microhardness measurement was performed on the nitrided surface (sample top), on the non-nitrided surface (sample bottom) and on the samples cross-section with a Shimadzu Micro Hardness Tester HMV-2T, applying a load of 10 gf to determine the microhardness profile (in the sample cross-section), and a load of 300 gf to determine the top and bottom hardness, for a peak-load contact of 15 s.

3. Results and Discussion

3.1. Surface and microstructural characterization

Figure 1 presents typical cross-section micrographs of the as-hardened, as-400°C-tempered and as-annealed samples nitrided for the different gas mixtures used here. As expected for the 350 °C nitriding temperature[51], the N (nitrogen)-chemically

Table 1. Plasma nitriding treatment conditions.

Samples code	Gas mixture (vol.%)	
#0	0% Ar + 100% (80% N_2 + 20% H_2)	80% N_2 + 20% H_2
#10	10% Ar + 90% (80% N_2 + 20% H_2)	10% Ar + 72% N_2 + 18% H_2
#20	20% Ar + 80% (80% N_2 + 20% H_2)	20% Ar + 64% N_2 + 16% H_2
#30	30% Ar + 70% (80% N_2 + 20% H_2)	30% Ar + 56% N_2 + 14% H_2
#40	40% Ar + 60% (80% N_2 + 20% H_2)	40% Ar + 48% N_2 + 12% H_2
#50	50% Ar + 50% (80% N_2 + 20% H_2)	50% Ar + 40% N_2 + 10% H_2

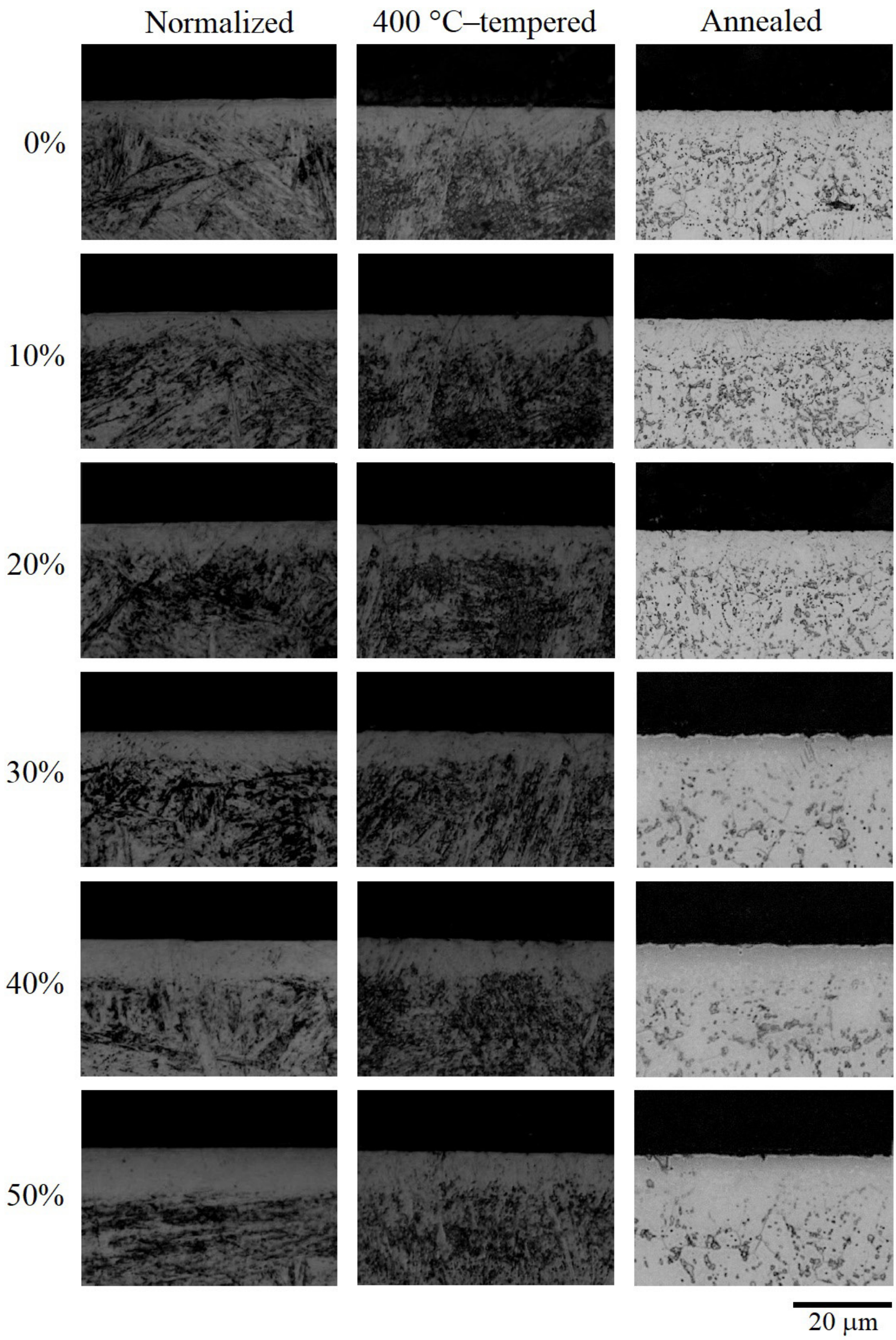

Figure 1. Cross-section micrographs of as-hardened, as-400 °C–tempered and as-annealed plasma nitrided AISI 420 steel samples treated under different argon content in gas mixture.

altered surface is not attacked or etched by the Villella's etchant while the N-unalloyed substrate bulk is etched. This result empirically indicates the greater resistance of the nitrided layer to acid corrosion than the original steel. The white-aspect layer occurrence suggests the nitrogen diffusion and nitrogen enrichment in interstitial solid solution on the body-centered cubic (bcc) or body-centered tetragonal (bct) structures, promoting the formation of the so-called expanded ferrite[55] and/or expanded martensite[56] phase, respectively. Another aspect worth highlighting is that no significant visual changes are observed among the nitrided layers obtained in the samples subjected to different prior heat treatments.

Figure 2a shows the XRD data of as-hardened samples for the untreated and nitrided condition as a function of the

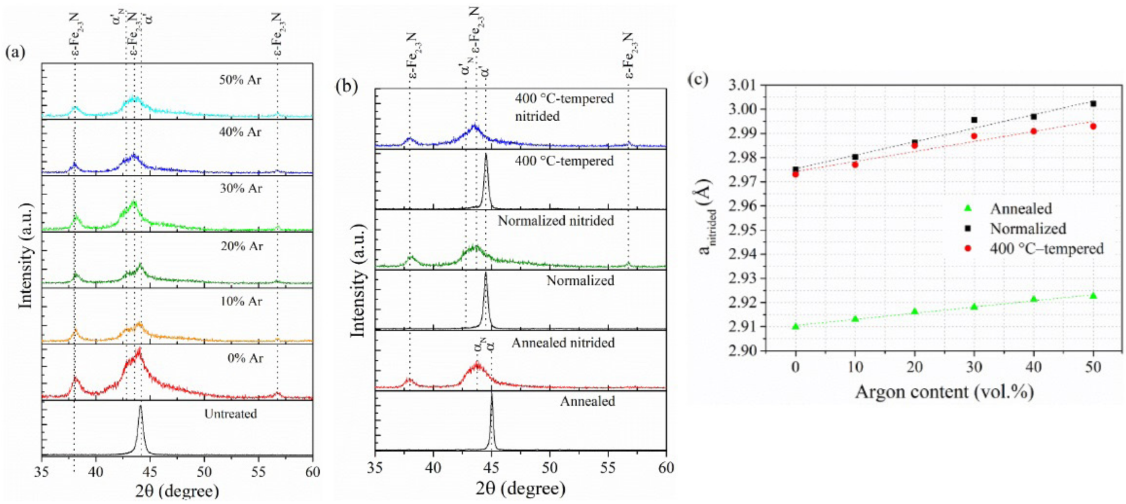

Figure 2. XRD patterns for: (a) as-hardened samples nitrided under different argon content in gas mixtures, (b) different samples pretreatment conditions and plasma nitrided under 50% argon content in the gas mixture, and (c) evolution of the lattice parameters on nitrided samples as a function of argon content in the gas mixture.

Ar content in the gas mixture. The untreated (as-hardened) sample presents on the adopted scan range (35-60°) the main (relative to 100% intensity) martensite phase (α′-Fe) peak. All post-nitrided as-hardened samples (which were in fact also simultaneously plasma tempered at 350 °C, as the nitriding treatment was carried out) show the formation of the nitrogen-expanded martensite (α'_N-Fe) and epsilon iron nitride (ε-$Fe_{2-3}N$) phase. As known, α'_N-Fe peak is usually identified on XRD data as broad peaks displaced to smaller 2θ angles, with greater interplanar distances when compared to the corresponding α'-Fe peak[57]. The α_N-Fe phase formation occurs as a result of deformation and consequent stress generation in the crystal lattice, due to nitrogen incorporation in solid solution[56]. As can be also seen from the Figure 2a analysis, the broader peaks also comprise contributions of ε-$Fe_{2-3}N$ precipitates, which exists for a large range of stoichiometry, comprised on ~25 to 33 at.% N, leading to overlapping peaks on the diffractogram[58].

Figure 2b shows a comparison between the XRD patterns of as-annealed, as-hardened and as-400°C-tempered, for untreated and treated samples at the 50% Ar + 50% (80% N_2 + 20% H_2) gas mixture (#50, in Table 1). From the comparison among nitrided as-hardened and as-400°C-tempered samples, it is noted that the former shows a higher intensity α'_N-Fe phase peak compared to the latter. This result can be attributed to the higher N solubility/supersaturation in the martensite lattice for the case of the as-hardened samples[53], which would be directly associated to the higher chromium content dissolved in solid solution and, theoretically, homogenously distributed all over the steel matrix. The nitrided as-annealed sample XRD pattern, in turn, shows the occurrence of the N-expanded ferrite phase (α_N-Fe), characterized by the broadened original ferrite (α-Fe) peak shifted to smaller angles[59-61], which confirms that the phase lattice parameter is increased by the N. The broadened peak feature is an indicative of the existence of N gradients occurring from the surface top into the substrate bulk that usually results in compressive residual stresses in the sample surface. In addition, no peaks related to the chromium nitride phases were identified, despite that second-phase particles in the form of chromium carbides are present in the as-annealed steel microstructure, as evidenced in the sample substrate bulk, in Figure 1. It is worth emphasizing that the absence of chromium nitrides and such second-phases rich in chromium (in the carbide form) at the sample surface could indicate that the treated material corrosion resistance was not affected. XRD data for the remaining evaluated conditions were not presented in this section, as they exhibit a similar pattern to that illustrated herein.

The lattice parameter (*a*) of the as-annealed, and as-400°C-tempered samples (both conditions showing *bcc* structure), and as-tempered samples (with *bct* structure), before and after nitriding, was determined using the obtained XRD data taken the plan (110) as reference. From this estimation, it was possible to obtain a comparative evaluation of the lattice expansion caused by the N diffusion under the indicated evaluated conditions. A deconvolution analysis of the XRD data of the nitrided samples for 2θ angles ranging from 41° to 46° was performed in order to more accurately determine the position of the α'_N-Fe (110) peak (see Table 2). Results indicated that the *a* lattice parameter increment, expressed in percentage values, for the *bct* structure of the as-hardened samples and those estimated for the as-400°C-tempered samples showing cubic martensite (*bcc*) phase post nitriding are similar, and agree well to those reported in the literature[51,56]. In contrast, the estimated values for the *bcc* structure of annealed samples post nitriding are far below the values reported in the literature for ferritic stainless steels (~ 5.24 for (110) plane)[60] and higher than those estimated for the ferrite phase present in nitrided super duplex stainless steel samples (~ 1.04% for (110) plane)[59]. It is believed that these differences are linked to variations in chemical composition between the compared alloys. Finally, as shown in Figure 2c, the lattice parameters ($a_{nitrided}$) of *bcc* and *bct*

Table 2. Experimental XRD data for 2θ peaks, the phase lattice parameter (a, being $a = d$ = interplanar distance) of the untreated substrate bulk ($2\theta_{matrix}$, a_{matrix}), and the nitrided surface ($2\theta_{nitrided}$, $a_{nitrided}$), and estimated variation (Δ) of the lattice parameter before (a_{matrix}) and after nitriding ($a_{nitrided}$), for the three distinct prior heat treatment (and the respective phase) conditions.

Condition		$2\theta_{matrix}$	$2\theta_{nitrided}$	a_{matrix} (Å)	$a_{nitrided}$ (Å)	$\Delta = a_{nitrided} - a_{matrix}$ (%)
#0	as-annealed (α-Fe)	44.68	43.97	2.86	2.909	1.745
(0% Ar)	as-hardened (α'_{bct}-Fe)	44.18	42.96	2.87-	2.974-	3.373-
	as-400°C-tempered (α'_{bcc}-Fe)	44.52	42.99	2.87	2.973	3.304
#10	as-annealed (α-Fe)	44.68	43.92	2.86	2.913	1.855
(10% Ar)	as-hardened (α'_{bct}-Fe)	44.18	42.88	2.87-	2.980-	3.557-
	as-400°C-tempered (α'_{bcc}-Fe)	44.52	42.93	2.87	2.976	3.442
#20	as-annealed (α-Fe)	44.68	43.87	2.86	2.916	1.965
(20% Ar)	as-hardened (α'_{bct}-Fe)	44.18	42.79	2.87-	2.986-	3.764-
	as-400°C-tempered (α'_{bcc}-Fe)	44.52	42.81	2.87	2.984	3.718
#30	as-annealed (α-Fe)	44.68	43.84	2.86	2.918	2.032
(30% Ar)	as-hardened (α'_{bct}-Fe)	44.18	42.65	2.87-	2.995-	4.089-
	as-400°C-tempered (α'_{bcc}-Fe)	44.52	42.75	2.87	2.988	3.857
#40	as-annealed (α-Fe)	44.68	43.79	2.86	2.921	2.142
(40% Ar)	as-hardened (α'_{bct}-Fe)	44.18	42.63	2.87-	2.996-	4.135-
	as-400°C-tempered (α'_{bcc}-Fe)	44.52	42.72	2.87	2.990	3.926
#50	as-annealed (α-Fe)	44.68	43.77	2.86	2.922	2.187
(50% Ar)	as-hardened (α'_{bct}-Fe)	44.18	42.55	2.87-	3.002-	4.322-
	as-400°C-tempered (α'_{bcc}-Fe)	44.52	42.69	2.87	2.992	3.996

structures of nitrided samples grow linearly with the addition of Ar content in the gas mixture.

Figure 3 shows nitrided layers thickness values as a function of the Ar content of the studied gas mixtures for the as-hardened, as-400°C-tempered, and as-annealed samples. It appears that the higher the Ar content the higher is the nitrided layer thickness. Likewise, it is possible to assert that a small variation in the thickness values was observed among the as-hardened, and as-400°C-tempered samples. In contrast, significantly smaller values were determined for the previously annealed samples. This behavior can be credited to the lower crystalline defect density present in the ferritic (α-Fe) structure, or its lower chromium content in solid solution, as it is expected due to the relatively intense chromium carbide precipitation dispersed all over the iron matrix, for the as-annealed condition. The previous heat treatment of hardening (applied for the other two heat treatment conditions studied here) leads to a higher crystalline defect density in the steel matrix structure, which constitutes high diffusivity paths favoring the nitrogen diffusion to greater depths[53]. Similarly, the higher chromium content dissolved in solid solution in both the martensitic matrixes (namely, the *bct* as well as the *bcc* one), due to the chromium carbide dissolution during the austenitization step of the hardening treatment, increases the nitrogen solubility[62]. Furthermore, the activation energy for the nitrogen diffusion in *bcc* structure for the annealed martensitic stainless steel (Q_α = 164 kJ mol^{-1})[62] is greater than in *bct* structure of as-hardened steel ($Q_{\alpha'}$ = 136 kJ mol^{-1})[63], leading to a lower nitrogen diffusivity and minor layer thickness.

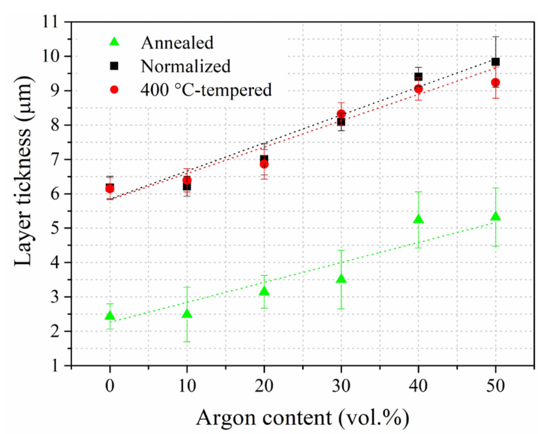

Figure 3. Evolution of the nitrided layer thickness as a function of argon content in the treated gas mixture.

The evolution of surface hardness as a function of Ar content in the gas mixture for as-annealed, as-hardened, and as-400°C-tempered samples is presented in Figure 4a. The hardness values clearly grow with the Ar content increase on the gas mixture. This behavior is linked both to the rise of nitrided layer thickness with the Ar increment, and the raise of N amount interstitially dissolved in α'_N-Fe phase allied to the presence of ε-$Fe_{2\text{-}3}N$ nitride phase in treated layers. The highest average hardness observed for the as-hardened condition is attributed to its higher crystalline defect density

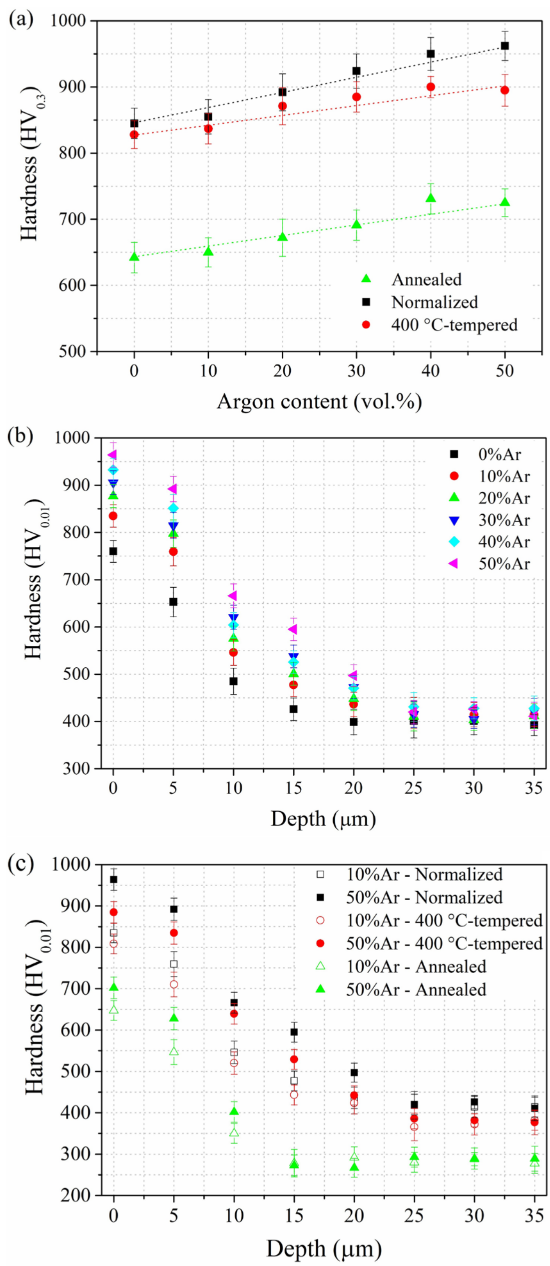

Figure 4. (a) Surface hardness and hardness profile for previous (b) as-hardened samples plasma nitrided under different argon content in gas mixtures, and (c) different samples pretreatment conditions and plasma nitrided under 10% and 50% argon content in the gas mixture.

favoring N diffusion. The impact of increasing crystal defects density on nitrogen diffusion kinetics and the efficiency of nitriding treatment has been demonstrated by several authors in the literature[64-68].

Figure 4b confirms the important role of Ar regarding the surface hardening. Note that the hardening depth is increased for nitrided as-hardened samples as the greater is the Ar content in the used gas mixture, within the studied values range. In addition, the smallest hardening depth occurs justly for the nitriding condition without the use of Ar in the gas mixture. In turn, Figure 4c, confronting the hardness profiles obtained for gas mixtures with 10 and 50 vol.% Ar, confirm the validity of this finding also for the nitrided as-400°C-tempered and as-annealed samples. It is worth highlighting that the increases observed in the thickness and hardness of the nitrided layer, as demonstrated in Figure 3 and Figure 4, are directly related to the formation of the phases identified in the XRD patterns presented in Figure 2.

Figure 5a shows the *Rz* and *Ra* roughness of the nitrided surfaces as a function of the Ar content used in the nitriding mixture. Results indicate roughness increase for all studied conditions as the Ar content is incremented. This result is related to the sputtering phenomenon caused by Ar-based species, in higher density in the plasma, as its content in the gas mixture is increased[15]. The obtained surface morphology after nitriding, as shown in Figure 5b (for *i*) as-hardened, *ii*) as-400°C-tempered; and *iii*) as-annealed samples), reveals the occurrence of a slight network, which seems to outline grain boundaries, an effect more evidenced for the as-annealed condition (Figure 5b(iii)). This morphology may be the consequence of the preferential nucleation and growth of iron nitrides along grains boundaries[69]. It is worth mentioning that here, it was not identified the transformation from lath- to plate-type martensite due to the enhancement of the martensite N content on the as-hardened and 400 °C–tempered nitrided samples, in disagreement to the evidenced for plasma carburized AISI 420 martensitic stainless steel samples, in ref[70].

3.2. Optical emission spectroscopy characterization

Figure 6 shows the brief of the optical emission spectroscopy results obtained for the analyzed 200-850 nm wavelength range. On the analyzed wavelength range, it was observed no significant signal for the ArH^+ (at 767.4 nm), H_2, H_2^+, H^+, and N^+ species in the abnormal glow discharge region. Results show the observed evolutions for the N_2, N_2^+, N, H, Ar^+ species, the later one occurring for the 763.51 nm wavelength. As expected, the Ar^+ density is increased for higher Ar contents, as expense of the decreased N- and H-based species densities in the gas mixture, which is supposedly related to the higher cross-section for the reaction (1), as follows[71]:

$$e^- + Ar \rightarrow e^- + e^- + Ar^+ \tag{1}$$

Regarding the atomic N-based species, which naturally are the main responsible by the successful of the samples nitriding, our optical emission spectroscopy results when confronted with our nitrided samples (surface and microstructural characterization) results, clearly indicate that the formation of atomic N species in the glow region of the obtained electrical discharges, due to the increased Ar contents, is not significant, since its density is decreased for higher Ar contents (strongly disagreeing with Figure 2 and Figure 4a results). This finding gives support for the assumption that atomic N-based species would preferentially be formed in profusion on the samples surface, from N_2-based species condensed at the treating

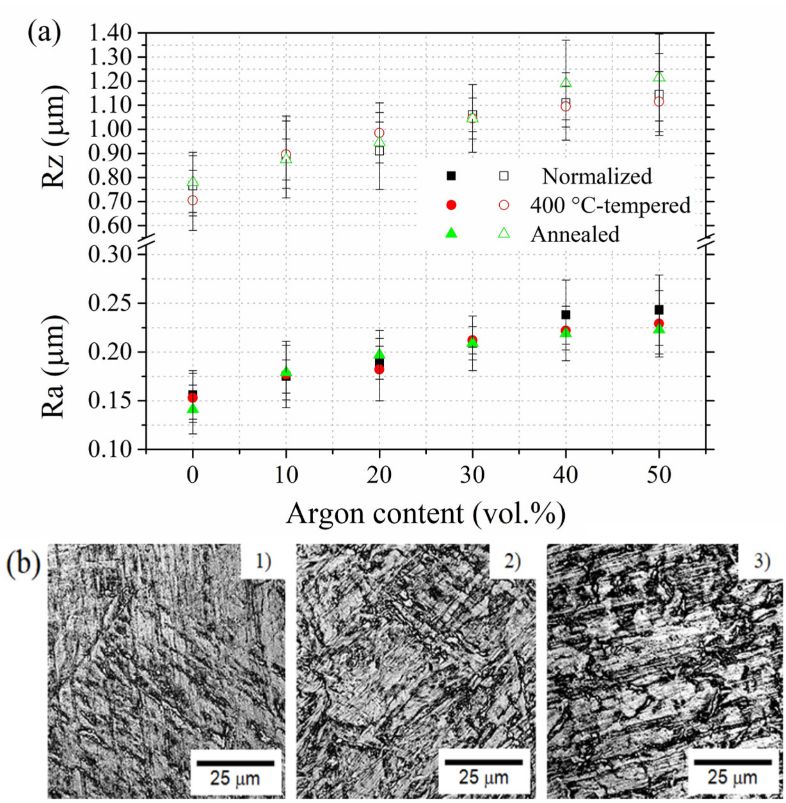

Figure 5. (a) Ra and Rz roughness and (b) surface morphology of 1) as-hardened, 2) as-400 °C–tempered and 3) as-annealed samples plasma nitrided under 50% argon content in the gas mixture.

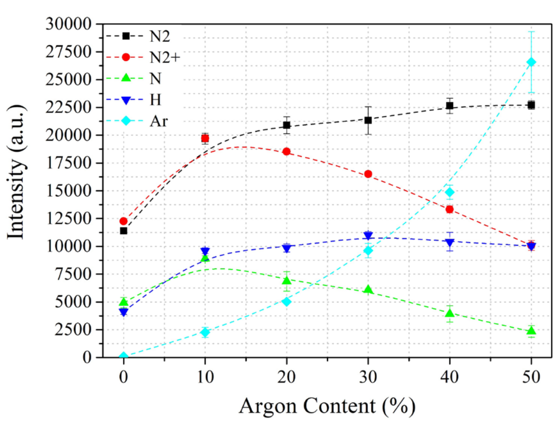

Figure 6. Optical emission spectroscopy results obtained for the analyzed 200-850 nm wavelength range.

surface, by thermal dissociation as well as by a dissociation intensified by the Ar-based fast species bombarding the treating surface. In other words, our successfully achieved nitrided surface features are due to the increment of the momentum transfer from Ar-based species at the samples surface as well as the increased atomic N chemical potential supplied for the steel treating surface, caused by the higher density of Ar-based fast (neutrals, excited and ions) plasma species bombarding the surface. As it is very well established that plasma nitriding is a diffusion-controlled treatment[51], despite the so expected diffusional limitation, since the treatment temperature and time was the same for all studied conditions, it can be also affirmed that the increased layer thickness and hardness observed in our Figure 2 and Figure 4a results are a consequence of the surface bombardment by a higher Ar-based species density, increasing the atomic N concentration in the outer superficial layer of the steel and the driving force for its diffusion, leading to a significant increment on the physical-chemical reactions (mainly sputtering, molecules dissociation and recombination) in surface-plasma interface, associated with the incremented higher-diffusivity paths present in the martensitic microstructures of the as-hardened and as-400°C-tempered samples.

4. Conclusion

Low-temperature plasma nitriding treatments were conducted using various N_2-H_2-Ar gas mixtures to assess the impact of Ar on glow discharge characteristics and surface properties of nitrided AISI 420 MSS samples. These samples underwent prior heat treatments including annealing, hardening, and hardening & 400°C tempering. The main conclusions of the study are summarized as follows:

- Low-temperature DC plasma nitriding in N_2-H_2-Ar gas mixtures effectively enhances the surface hardness of AISI 420 steel samples. This hardness improvement results from the formation of a nitrided layer comprising ε-$Fe_{2-3}N$ iron nitride and nitrogen-expanded phases.

- The previous heat treatment has proven to be a crucial parameter in the plasma nitriding treatment of steels exhibiting metastable phases. From the same base material, the mechanical properties of the resulting modified surface can only be altered through careful selection of the preceding heat treatment.
- For the conditions examined, the rise in Ar content within the assessed range led to an increase in nitride layer thickness. Surface hardness and roughness likewise increased accordingly.
- Hardness profile measurements reveal a smoothed interface between the nitrided layer and the bulk, indicating a hardening depth of approximately 20 µm for both the nitrided as-hardened and as-hardened & 400°C-tempered samples, and approximately 10 µm for the as-annealed samples.

5. Acknowledgments

This work was supported by CAPES (Coordenação de Aperfeiçoamento de Pessoal de Nível Superior–Brasil–Finance Code 001), CNPq (Conselho Nacional de Desenvolvimento Científico e Tecnológico), CNPq-Universal Grant N. 482380/2012-8, MCTI/CNPq/CT-Aquaviário Grant N. 456347/2013-5 and Fundação Araucária do Estado do Paraná (PRONEX - Grant N. 46744). Dr. M. Mafra thanks to CNPq by the financial support through Process n. 311716/2018-0. Dr. C.J. Scheuer thanks to FAPERGS (Research Support Foundation of the Rio Grande do Sul State) by the financial support through Grant N. 19/2551-0001749-9, and CNPq (Conselho Nacional de Desenvolvimento Científico e Tecnológico) through Grant No. 309675/2022-7. The authors also wish to express thanks to the Laboratory of X-ray Optics and Instrumentation – LORXI, by the use of the X-ray diffraction equipment, and Additive Manufacturing and Surface Engineering Laboratory – LAMSE, by the use of the confocal laser scanning microscope equipment, both laboratories from the Universidade Federal do Paraná (UFPR).

6. References

1. Borgioli F. The “expanded” phases in the low-temperature treated stainless steels: a review. Metals. 2022;12(2):331. http://doi.org/10.3390/met12020331.
2. Somers MAJ, Christiansen TL. Nitriding of steels. In: Caballero FG, editor. Encyclopedia of materials: metals and alloys. Amsterdam: Elsevier; 2022. p. 173-89. http://doi.org/10.1016/B978-0-12-819726-4.00036-3.
3. Berladir K, Hovorun T, Ivanov V, Vukelic D, Pavlenko I. Diffusion nitride coatings for heat-resistant steels. Materials. 2023;16(21):6877. http://doi.org/10.3390/ma16216877.
4. Sun J, Li J, Xie JM, Yang Y, Wu WP, Zhou X, et al. Properties of rapid arc discharge plasma nitriding of AISI 420 martensitic stainless: effect of nitriding temperatures. J Mater Res Technol. 2022;19:4804-14. http://doi.org/10.1016/j.jmrt.2022.07.028.
5. Sharma MK, Saikia BK, Phukan A, Ganguli B. Plasma nitriding of austenitic stainless steel in N_2 and N_2–H_2 dc pulsed discharge. Surf Coat Tech. 2006;201(6):2407-13. http://doi.org/10.1016/j.surfcoat.2006.04.006.
6. Almeida EAS, Milan JCG, Costa CE. Acquired properties comparison of solid nitriding, gas nitriding and plasma nitriding in tool steels. Mater Res. 2015;18(1):27-35. http://doi.org/10.1590/1516-1439.255513.
7. Umemura MT, Varela LB, Pinedo CE, Cozza RC, Tschiptschin AP. Assessment of tribological properties of plasma nitrided 410S ferritic-martensitic stainless steels. Wear. 2019;426:49-58. http://doi.org/10.1016/j.wear.2018.12.092.
8. Scheuer CJ, Cardoso RP, Brunatto SF. An overview on plasma-assisted thermochemical treatments of martensitic stainless steels. Surf Topogr. 2023;1(1):013001. http://doi.org/10.1088/2051-672X/acb372.
9. Ferreira LM, Brunatto SF, Cardoso RP. Martensitic stainless steels low-temperature nitriding: dependence of substrate composition. Mater Res. 2015;18(3):622-7. http://doi.org/10.1590/1516-1439.015215.
10. Dalibon E, Charadia R, Cabo A, Brühl SP. Short time ion nitriding of AISI 420 martensitic stainless steel to improve wear and corrosion resistance. Mater Res. 2019;22(6):e20190415. http://doi.org/10.1590/1980-5373-mr-2019-0415.
11. Moskalioviene T, Galdikas A. Mechanisms of the hydrogen influence on the diffusivity of nitrogen during plasma nitriding austenitic stainless steel. Metall Mater Trans, A Phys Metall Mater Sci. 2019;50(2):1021-32. http://doi.org/10.1007/s11661-018-5014-4.
12. Latif H, Saeed A, Rana SJ, Khan BS, Hayat SS. Nitrogen dissociation and its excitation/vibrational temperature with hydrogen admixture in 50 Hz DC discharge. Radiat Eff Defects Solids. 2017;172(11-12):1-15. http://doi.org/10.1080/10420150.2017.1413648.
13. Skonieski AFO, Lima ES, Hirsch T, Rocha AS. Influência da mistura gasosa em processos de nitretação e nitrocarbonetação a plasma. Rev Bras Apl Vac. 2008;27:175-82. http://doi.org/10.17563/rbav.v27i4.469.
14. Naeem M, Khan KH, Shahid M, Shafiq JIM, Zaka-ul-Islam M, Zakaullah M. Non-intrusive measurement of electron, vibrational, rotational temperatures and active species concentration in N_2-H_2 cathodic cage plasma. Surf Coat Tech. 2018;344:233-43. http://doi.org/10.1016/j.surfcoat.2018.03.024.
15. Allenstein AN, Cardoso RP, Machado KD, Weber S, Pereira KMP, Santos CAL, et al. Strong evidences of tempered martensite- to-nitrogen-expanded austenite transformation in CA-6NM steel. Mater Sci Eng A. 2012;552:569-72. http://doi.org/10.1016/j.msea.2012.05.075.
16. Naeem M, Iqbal J, Abrar M, Khan KH, Díaz-Guillén JC, Lopez-Badillo CM, et al. The effect of argon admixing on nitriding of plain carbon steel in N_2 and N_2-H_2 plasma. Surf Coat Tech. 2018;350:48-56. http://doi.org/10.1016/j.surfcoat.2018.07.004.
17. Priest JM, Baldwin MJ, Fewell MP. The action of hydrogen in low-pressure r.f.-plasma nitriding. Surf Coat Tech. 2001;145(1-3):152-63. http://doi.org/10.1016/S0257-8972(01)01311-1.
18. Brunatto SF, Muzart JLR. Influence of the gas mixture flow on the processing parameters of hollow cathode discharge iron sintering. J Phys D Appl Phys. 2007;40(13):3937-44. http://doi.org/10.1088/0022-3727/40/13/005.
19. Moradshahi M, Tavakoli T, Amiri S, Shayeganmehr S. Plasma nitriding of Al alloys by DC glow discharge. Surf Coat Tech. 2006;201(1-3):567-74. http://doi.org/10.1016/j.surfcoat.2005.12.002.
20. Matsumoto O, Konuma M, Yasushi K. Nitriding of titanium in an r.f. discharge II: effect of the addition of hydrogen to nitrogen on nitriding. J Less Common Met. 1982;84:157-63. http://doi.org/10.1016/0022-5088(82)90141-2.
21. Avni R, Spalvins T. Nitriding mechanisms in ArN_2, ArN_2H_2 and $ArNH_3$ mixtures in D.C. Glow discharges at low pressures.

Mater Sci Eng. 1987;95:237-46. http://doi.org/10.1016/0025-5416(87)90515-5.
22. Edenhofer B. Physical and metallurgical aspects of ionitriding - part 2. Heat. Treat. Met. 1974;2:59-67.
23. Sun Y, Bell T. Plasma surface engineering of low alloy steel. Mater Sci Eng A. 1991;140:419-34. http://doi.org/10.1016/0921-5093(91)90458-Y.
24. Alsaran A, Karakan M, Celik A. The investigation of mechanical properties of ion-nitrided AISI 5140 low-alloy steel. Mater Charact. 2002;48(4):323-7. http://doi.org/10.1016/S1044-5803(02)00275-9.
25. Alsaran A, Celik A, Çelik C. Determination of the optimum conditions for ion nitriding of AISI 5140 steel. Surf Coat Tech. 2002;160(2-3):219-26. http://doi.org/10.1016/S0257-8972(02)00401-2.
26. Sousa RRM, Araújo FO, Gontijo LC, Costa JAP, Alves C Jr. Cathodic cage plasma nitriding (CCPN) of austenitic stainless steel (AISI 316): influence of the different ratios of the (N_2/H_2) on the nitrided layers properties. Vacuum. 2012;86(12):2048-53. http://doi.org/10.1016/j.vacuum.2012.05.008.
27. Kumar S, Baldwin MJ, Fewell MP, Haydon SC, Short KT, Collins GA, et al. The effect of hydrogen on the growth of the nitrided layer in r.f.-plasma-nitrided austenitic stainless steel AISI 316. Surf Coat Tech. 2000;123(1):29-35. http://doi.org/10.1016/S0257-8972(99)00393-X.
28. Lepienski CM, Nascimento FC, Foerster CE, Silva SLR, Siqueira CJM, Alves C Jr. Glow discharge nitriding in AISI 304 at different nitrogen–hydrogen atmospheres: structural, mechanical and tribological properties. Mater Sci Eng A. 2008;489(1-2):201-6. http://doi.org/10.1016/j.msea.2007.12.012.
29. Negm NZ. Effect of annealing temperature on properties of H_2/N_2 rf plasma-treated stainless steel. Surf Coat Tech. 2006;201(3-4):1763-7. http://doi.org/10.1016/j.surfcoat.2006.03.003.
30. Amiri S, Moradshahi M. Influence of different layer microstructures induced by different gas compositions on corrosion behavior of plasma nitrided stainless steel. Surf Coat Tech. 2007;201(16-17):7375-81. http://doi.org/10.1016/j.surfcoat.2007.02.006.
31. Tamaki M, Tomii Y, Yamamoto N. The role of hydrogen in plasma nitriding: hydrogen behavior in the titanium nitride layer. Plasmas & Ions. 2000;3(1-4):33-9. http://doi.org/10.1016/S1288-3255(00)00108-8.
32. Allenstein AN, Lepienski CM, Buschinelli AJA, Brunatto SF. Plasma nitriding of CA-6NM steel: effect of H2 + N2 gas mixtures in nitride layer formation for low N2 contents at 500 °C. Mater Res. 2010;1(4):557-62. http://doi.org/10.1590/S1516-14392010000400020.
33. Karakan M, Alsaran A, Celik A. Effects of various gas mixtures on plasma nitriding behavior of AISI 5140 steel. Mater Charact. 2002;49(3):241-6. http://doi.org/10.1016/S1044-5803(03)00010-X.
34. Fancey KS. An investigation into dissociative mechanisms in nitrogenous glow discharges by optical emission spectroscopy. Vacuum. 1995;46(7):695-700. http://doi.org/10.1016/0042-207X(94)00146-4.
35. Fancey KS, Leyland A, Egerton D, Torres D, Matthews A. The influence of process gas characteristics on the properties of plasma nitrided steel. Surf Coat Tech. 1995;76-77:694-9. http://doi.org/10.1016/0257-8972(96)80008-9.
36. Reyes P, Torres C, Martínez H. Electron temperature and ion density measurements in a glow discharge of an Ar–N_2 mixture. Radiat Eff Defects Solids. 2014;169(4):285-92. http://doi.org/10.1080/10420150.2013.860975.
37. Naeem M, Zaka-ul-Islam M, Khattak ZI, Shafiq M, Zakaullah M. Influence of argon fraction on plasma parameters in H_2-N_2 mixture discharge with cathodic cage. Eur Phys J Appl Phys. 2017;7(1):10801. http://doi.org/10.1051/epjap/2016160280.
38. Saloum S, Naddaf M, Alkhaled B. Diagnostics of N_2–Ar plasma mixture excited in a 13.56 MHz hollow cathode discharge system: application to remote plasma treatment of polyamide surface. J Phys D Appl Phys. 2008;41(4):045205. http://doi.org/10.1088/0022-3727/41/4/045205.
39. Rehman NU, Anjum Z, Masood A, Farooq M, Ahmad I, Zakaullah M. Metrology of non-thermal capacitively coupled N2–Ar mixture plasma. Opt Commun. 2013;296:72-8. http://doi.org/10.1016/j.optcom.2013.01.004.
40. Song MA, Lee YW, Chung TH. Characterization of an inductively coupled nitrogenargon plasma by Langmuir probe combined with optical emission spectroscopy. Phys Plasmas. 2011;18(2):023504. http://doi.org/10.1063/1.3554706.
41. Itagaki N, Iwata S, Muta K, Yonesu A, Kawakami S, Ishii N, et al. Electron temperature dependence of nitrogen dissociation in 915 MHz ECR plasma. Thin Solid Films. 2003;435(1-2):259-63. http://doi.org/10.1016/S0040-6090(03)00395-X.
42. Ikhlaq U, Ahmad R, Saleem S, Shah MS, Umm-i-Kalsoom N, Khan N, et al. Argon gas concentration effects on nanostructured molybdenum nitride layer growth using 100 Hz pulsed dc glow discharge. Eur Phys J Appl Phys. 2012;59(2):20801. http://doi.org/10.1051/epjap/2012120173.
43. Ikhlaq U, Hirose A, Ahmad R, Ikhlaq A, Saleem S, Sammynaiken R, et al. The role of Ar flow rates on synthesis of nanostructured zirconium nitride layer growth using plasma enhanced hot filament nitriding (PEHFN) technique. Eur Phys J Appl Phys. 2015;69(1):10801. http://doi.org/10.1051/epjap/2014140246.
44. Fancey KS, Leyland A, Egerton D, Torres D, Matthews A. The influence of process gas characteristics on the properties of plasma nitrided steel. Surf Coat Tech. 1995;76-77:694-9. http://doi.org/10.1016/0257-8972(96)80008-9.
45. Farayibi PK, Hankel J, van gen Hassend F, Blüm M, Weber S, Röttger A. Tribological characteristics of sintered martensitic stainless steels by nano-scratch and nanoindentation tests. Wear. 2023;512–513:204547. http://doi.org/10.1016/j.wear.2022.204547.
46. Scheuer CJ, Silva LJ, Neves JCK, Cardoso RP, Brunatto SF. Tribological performance of low-temperature plasma carburized AISI 420 martensitic stainless steel. Surf Coat Tech. 2024;476:130239. http://doi.org/10.1016/j.surfcoat.2023.130239.
47. Mainardi VA, Cardoso RP, Brunatto SF, Scheuer CJ. Tribocorrosion behavior of low-temperature plasma-carburized AISI 420 martensitic stainless steel: investigating the synergy between corrosion and erosion in slurry and liquid impingement environments. Surf Coat Tech. 2024;477:130373. http://doi.org/10.1016/j.surfcoat.2024.130373.
48. Mainardi VA, Cardoso RP, Brunatto SF, Scheuer CJ. Slurry and liquid impingement erosion behavior of low-temperature plasma carburized AISI 420 martensitic stainless steel. Surf Coat Tech. 2024;477:130390. http://doi.org/10.1016/j.surfcoat.2024.130390.
49. Scheuer CJ, Zanetti FI, Cardoso RP, Brunatto SF. Ultra-low-to hightemperature plasma-assisted nitriding: revisiting and going further on the martensitic stainless steel treatment. Mater Res Express. 2018;6(2):026529. http://doi.org/10.1088/2053-1591/aaeca2.
50. Scheuer CJ, Cardoso RP, Brunatto SF. Sequential low-temperature plasma-assisted thermochemical treatments of the AISI 420 martensitic stainless steel. Surf Coat Tech. 2021;421:127459. http://doi.org/10.1016/j.surfcoat.2021.127459.
51. Lima JFV, Scheuer CJ, Brunatto SF, Cardoso RP. Kinetics of the UNS S32750 super duplex stainless steel low-temperature plasma nitriding. Mater Res. 2022;25:e20210463. http://doi.org/10.1590/1980-5373-mr-2021-0463.
52. Scheuer CJ, Cardoso RP, Mafra M, Brunatto MSF. Effects of the voltage and pressure on the carburizing of martensitic stainless steel in pulsed DC glow discharge. Mater Res. 2021;24(6):e20210154. http://doi.org/10.1590/1980-5373-mr-2021-0154.
53. Cardoso RP, Scheuer CJ, Brunatto SF. Low-temperature nitriding kinetics of stainless steel: effect of prior heat treatment. In: Colás R, Totten GE, editors. Encyclopedia of iron, steel, and

their alloys. Boca Raton: CRC Press; 2016. p. 2153-68. http://doi.org/10.1081/E-EISA-120051669.
54. Anjos AD, Scheuer CJ, Brunatto SF, Cardoso RP. Low-temperature plasma nitrocarburizing of the AISI 420 martensitic stainless steel: microstructure and process kinetics. Surf Coat Tech. 2015;275:51-7. http://doi.org/10.1016/j.surfcoat.2015.03.039.
55. Sousa RS, Araújo FO, Costa JAP, Oliveira AM, Melo MS, Alves C Jr. Cathodic cage nitriding of AISI 409 ferritic stainless steel with the addition of CH4. Mater Res. 2012;15(2):260-5. http://doi.org/10.1590/S1516-14392012005000016.
56. Kim SK, Yoo JS, Priest JM, Fewell MP. Characteristics of martensitic stainless steel nitrided in a low-pressure RF plasma. Surf Coat Tech. 2003;163-164:380-5. http://doi.org/10.1016/S0257-8972(02)00631-X.
57. Li Y, Zhang S-Z, Qiu J-X, He Y-Y, Xiu J-J, Ye Q-W, et al. Effect of electric potentials on microstructure, corrosion and wear characteristic of the nitrided layer prepared on 2Cr13 stainless steel by plasma nitriding. Acta Metall Sin. 2019;32:733-45.
58. Li J, Tao X, Wu W, Xie G, Yang Y, Zhou X, et al. Effect of arc current on the microstructure, tribological and corrosion performances of AISI 420 martensitic stainless steel treated by arc discharge plasma nitriding. J Mater Sci. 2023;58(5):2294-309. http://doi.org/10.1007/s10853-023-08161-8.
59. Kurelo BCES, Souza GB, Serbena FC, Lepienski CM, Borges PC. Mechanical properties and corrosion resistance of αN-rich layers produced by PIII on a super ferritic stainless steel. Surf Coat Tech. 2020;403:126388. http://doi.org/10.1016/j.surfcoat.2020.126388.
60. Luiz LA, Kurelo BCES, Souza GB, Andrade J, Marino CEB. Effect of nitrogen plasma immersion ion implantation on the corrosion protection mechanisms of different stainless steels. Mater Today Commun. 2021;28:102655. http://doi.org/10.1016/j.mtcomm.2021.102655.
61. Araújo E, Bandeira RM, Manfrinato MD, Moreto JA, Borges R, Vales SDS, et al. Effect of ionic plasma nitriding process on the corrosion and micro-abrasive wear behavior of AISI 316L austenitic and AISI 470 super-ferritic stainless steels. J Mater Res Technol. 2019;8(2):2180-91. http://doi.org/10.1016/j.jmrt.2019.02.006.
62. Casteletti LC, Lombardi A No, Totten GE. Nitriding of stainless steels. Metallogr. Microstruct. Anal. 2014;3(6):477-508. http://doi.org/10.1007/s13632-014-0170-4.
63. Scheuer CJ, Cardoso RP, Brunatto SF. Low-temperature plasma assisted thermochemical treatments of AISI 420 steel: comparative study of obtained layers. Mater Res. 2015;18(6):1392-9. http://doi.org/10.1590/1516-1439.013815.
64. Wen K, Zhang C, Gao Y. Influence of gas pressure on the low-temperature plasma nitriding of surface-nanocrystallined TC4 titanium alloy. Surf Coat Tech. 2022;436:128327. http://doi.org/10.1016/j.surfcoat.2022.128327.
65. Xu C, Wang X, Zhang B, Luo X, Tang Z, Dai S. Effect of the pre-shot peening and nitrogen ion implantation combined surface treatments on the surface structure and properties of gear steel 16Cr3NiWMoVNbE. Metals. 2022;12(9):1509. http://doi.org/10.3390/met12091509.
66. Xiao H, Liu X, Lu Q, Hu T, Hong Y, Li C, et al. Promoted low-temperature plasma nitriding for improving wear performance of arc-deposited ceramic coatings on Ti6Al4V alloy via shot peening pretreatment. J Mater Res Technol. 2022;19:2981-90. http://doi.org/10.1016/j.jmrt.2022.06.067.
67. Bai Z, Wu X. Improving stress corrosion resistance and wear resistance of austenitic hot-stamping die steels via synergistic effects of shot peening and plasma nitriding. Surf Coat Tech. 2024;478:130448. http://doi.org/10.1016/j.surfcoat.2024.130448.
68. E Dib J, Gómez B, Strubbia R, Ares A, Méndez C, Fuster V, et al. Characterization of plasma nitrided duplex stainless steel: influence of prior shot peening and nitriding atmosphere. J Mater Eng Perform. 2023;32(1):406-14. http://doi.org/10.1007/s11665-022-07076-w.
69. Keddam M. Characterization of the nitrided layers of XC38 carbon steel obtained by R.F. plasma nitriding. Appl Surf Sci. 2008;254(8):2276-80. http://doi.org/10.1016/j.apsusc.2007.09.012.
70. Brunatto SF, Scheuer CJ, Boromei I, Martini C, Ceschini L, Cardoso RP. Martensite coarsening in low-temperature plasma carburizing. Surf Coat Tech. 2018;350:161-71. http://doi.org/10.1016/j.surfcoat.2018.07.002.
71. Chapman B. Glow discharge processes. New York: John Wiley & Sons; 1980.